Modular Entropy Retrieval in Black-Hole Information Recovery: A Proper-Time Saturation Model

Evlondo Cooper *

Posted Date: 18 June 2025

doi: 10.20944/preprints202503.2057.v5

Keywords: black hole information paradox; observer-dependent entropy; Rényi entropy; entanglement wedge reconstruction; quantum information; physics

 doi:10.20944/preprints202503.2057.v5

Article

Modular Entropy Retrieval in Black-Hole Information Recovery: A Proper-Time Saturation Model

Evlondo Cooper

Independent Researcher, USA

Abstract: We derive a proper-time–dependent entropy-retrieval law stating that the growth rate of retrievable entropy is proportional to the remaining entropy gap, modulated by a hyperbolic-tangent regulator that switches on at a characteristic proper time τ_{char}. Unlike phenomenological fits to the Page curve, this law follows directly from bounded Tomita–Takesaki modular flow and is fully invertible from simulated or empirical retrieval curves. The framework converts global entropy conservation into a Lorentzian-causal, observer-specific recovery process. It predicts distinct trajectories for stationary, freely falling, and accelerated observers and yields an acceleration-indexed $g^{(2)}(t_1, t_2)$ envelope that Bose–Einstein–condensate analog black holes can measure on 10–100 ms timescales. Numerical validation on a 48-qubit MERA lattice (bond dimension 8) confirms robustness; a modified Ryu–Takayanagi prescription embeds the model in AdS/CFT without replica-wormhole or island constructions. By replacing ensemble-averaged Page curves with a causal, falsifiable mechanism, the model reframes the black-hole information paradox as an experimentally accessible dynamical question. Here $S_{\max}$ is the Bekenstein–Hawking entropy, $\gamma(\tau)$ is the modular-flow retrieval rate, and τ_{char} sets the characteristic proper-time scale.

Keywords: black-hole entropy paradox; Tomita–Takesaki modular flow; observer-dependent entropy; Rényi entropy; entanglement-wedge reconstruction; analog black-hole gravity; $g^{(2)}$ correlations

1. Introduction

Entropy without Access

The black-hole information paradox persists not because information is lost, but because no existing framework retrieves it causally. Replica–wormhole paths [1,2], island prescriptions [3], ensemble Page–curve models [4,5], and ER = EPR dualities [6] all reproduce the required fine-grained entropy curves, yet none supplies a Lorentzian, proper-time recovery channel that delivers the state to a detector. Stabilizing entropy without a causal retrieval channel leaves the paradox unresolved at the operational level.

Key assumptions. (i) modular spectra are regulator bounded by standard split inclusions; (ii) modular flow is treated semiclassically on fixed backgrounds; (iii) present BEC analog systems resolve $g^{(2)}$ down to approximately 2 ms.

1.1. Operational–Access Criterion

A framework resolves the paradox only if it meets all of the following conditions:

(a) **Proper-time delivery**: specifies how entropy reaches an observer as proper time unfolds;
(b) **Lorentzian grounding**: roots that access in Lorentzian causality;
(c) **First-principles derivation**: derives the process from accepted QFT or GR principles rather than retrospective fitting;

 doi:10.20944/preprints202503.2057.v5

(d) **Empirical testability**: predicts observer-dependent lags $\Delta\tau$ within sub-exponential resource bounds[1].

Table 1. Compliance of major black-hole information proposals with the criteria in Section 1.1. A check mark denotes compliance; a cross denotes failure.

Framework	(a)	(b)	(c)	(d)
Replica wormholes	×	×	✓	×
Islands	×	×	✓	×
Ensemble Page	×	✓	×	×
ER=EPR	×	✓	×	×

Each proposal satisfies at most two criteria; none supplies a causal, observer-accessible retrieval channel. Resolution therefore demands an explicit recovery law derivable in proper time, grounded in Lorentzian causality, and testable within polynomial resources. The Observer-Dependent Entropy Retrieval (ODER) framework meets those demands with modular-flow dynamics and wedge-reconstruction depths that scale polynomially, in contrast with the exponential-cost Hayden–Preskill decoder $\mathcal{O}(2^n)$ assumed for global recovery. This reframes the paradox not as a global entropy-balancing problem, but as a concrete question of when, and whether, retrieval occurs for a specific observer. Entropy accounting differs from information access; analytic continuation does not define temporal evolution; and reconstruction alone does not constitute recovery.

Reader guide

- Section 2 derives the observer-indexed retrieval law and presents an inverse map that reconstructs $\gamma(\tau)$ from measured $S_{\text{ret}}(\tau)$.
- Section 6 validates the law on a 48-qubit MERA lattice, establishing the $\mathcal{O}(n \log n)$ scaling.
- Section 7.5 translates the theory into the $g^{(2)}$ fringe measurable in current BEC analogs.
- Section 4.1 provides a calibration protocol for τ_{char}.
- Section 7.4 defines the retrieval–evaporation gap Δ_{fail}.

Appendix E offers an interpretive correspondence for readers unfamiliar with modular dynamics, mapping $\gamma(\tau)$, τ_{char}, and Δ_{fail} to gravitationally intuitive quantities without altering the retrieval framework.

Code, data, and figure-generation notebooks are archived at https://doi.org/10.5281/zenodo.15428312.

2. Observer-Dependent Entropy Retrieval

Novel Framework.

ODER treats recovery as a dynamical, observer-indexed process and employs the unique tanh onset that, as proved in Theorem A.2, is the only profile compatible with bounded modular spectra and Paley–Wiener causality. This section derives

$$\frac{dS_{\text{retr}}}{d\tau} = \gamma(\tau)[S_{\max} - S_{\text{retr}}(\tau)] \tanh\big(\tau/\tau_{\text{char}}\big), \tag{1}$$

directly from Tomita–Takesaki modular flow on nested von Neumann algebras.

Because Eq. (1) is first order and monotone in $S_{\text{retr}}(\tau)$, we can solve it for the unknown rate $\gamma(\tau)$. This inversion is essential in Section 3, where retrieval rates for different observer classes are compared.

[1] Sub-exponential relative to decoding complexity; for example circuit depth or modular-spectrum reconstruction.

 doi:10.20944/preprints202503.2057.v5

$$\boxed{\gamma(\tau) = \frac{1}{\left[S_{\max} - S_{\mathrm{retr}}(\tau)\right] \tanh\left(\tau/\tau_{\mathrm{char}}\right)} \frac{dS_{\mathrm{retr}}}{d\tau}} \qquad \text{(Inverse retrieval map)}$$

Implication. Once an experiment measures $S_{\mathrm{retr}}(\tau)$, for example through the $g^{(2)}$ fringe, the boxed map fixes $\gamma(\tau)$ without further assumptions, turning ODER from a forward model into a calibratable decoder.

Goal	model entropy recovery as a bounded, causal convergence in proper time that differs by observer.
Mechanism	Eq. (1) depends on modular-spectrum gradients. $\gamma(\tau)$ encodes redshift, Unruh, or interior-correlation effects.
Domain of validity	algebraic QFT on Lorentzian backgrounds. Simulations on a 48-qubit MERA lattice confirm robustness. The model predicts an acceleration-dependent $g^{(2)}$ envelope in BEC analog black holes on 10–100 ms timescales, a signature absent from non-retrieval models.

We define the retrieval horizon

$$\tau_{\mathrm{RH}} := \inf\left\{\tau \,\middle|\, S_{\mathrm{retr}}(\tau) \geq 0.9\, S_{\max}\right\},$$

the proper time at which 90% of the retrievable entropy is accessed; this horizon is distinct from both the entanglement wedge and the classical event horizon.

Self-Audit: ODER Failure Modes

- **Modular realism:** modular Hamiltonians must remain physical in strong-gravity regimes.
- **Simulation abstraction:** MERA results may drift for large bond dimension, so convergence must be checked.
- **Empirical anchoring:** analog experiments must isolate modular-flow signatures from background noise.
- **Complexity barrier:** an exact digital decoder may still require exponential resources.
- **Uniqueness risk:** future QECC or monitored-circuit frameworks may yield rival retrieval laws.

Astrophysical forecast.

For a solar-mass Schwarzschild black hole, Eq. (1) implies that a stationary observer at $r = 10\,GM/c^2$ retrieves at least 90% of the missing entropy only after $\sim 10^{67}$ yr, a timescale absent from replica-wormhole or island prescriptions. Sections 6–7.5 benchmark the law and outline experimental validation, showing that information is not lost but modularly retrieved on observer-specific clocks.

3. Observer-Dependent Entropy in Curved Spacetime

We classify three canonical observer trajectories and track entropy-retrieval dynamics along each. The retrieval rate $\gamma(\tau)$ is fixed by the local modular Hamiltonian, with no phenomenological fits, and evolves with proper time.

3.1. Classification of Observers

Stationary observer.

A detector at fixed radius $r > 2M$ perceives Hawking radiation as redshifted thermal flux; this gives

$$\gamma_{\mathrm{stat}}(\tau) \propto \frac{1}{r}, \tag{2}$$

and a monotonic decay in $g^{(2)}$ correlations. For $r = 10\,M$ we find $\tau_{\mathrm{char}} < \tau_{\mathrm{Page}}$ because no interior mode enters the algebra.

 doi:10.20944/preprints202503.2057.v5

Freely falling observer.

A geodesic world line crosses the horizon at τ_{cross}; interior modes then boost the retrieval rate,

$$\gamma_{\text{fall}}(\tau) \gg \gamma_{\text{stat}}(\tau), \quad \tau > \tau_{\text{cross}}, \tag{3}$$

accelerating saturation (orange curve in Figure 1).

Accelerating observer.

A uniformly accelerating detector experiences both Hawking and Unruh flux,

$$\gamma_{\text{eff}}(\tau, a) = \gamma_{\text{Hawking}}(\tau) + \gamma_{\text{Unruh}}(\tau, a), \tag{4}$$

with $\gamma_{\text{Unruh}} \propto a^2$ [12]. At $a = 0.2\,c^2/M$ the retrieval envelope is the green curve in Figure 1.

Experimental emulation: stationary and accelerating channels can be engineered in waterfall BECs, while freely falling trajectories correspond to time-of-flight release [13]. Parameters appear in Table 2.

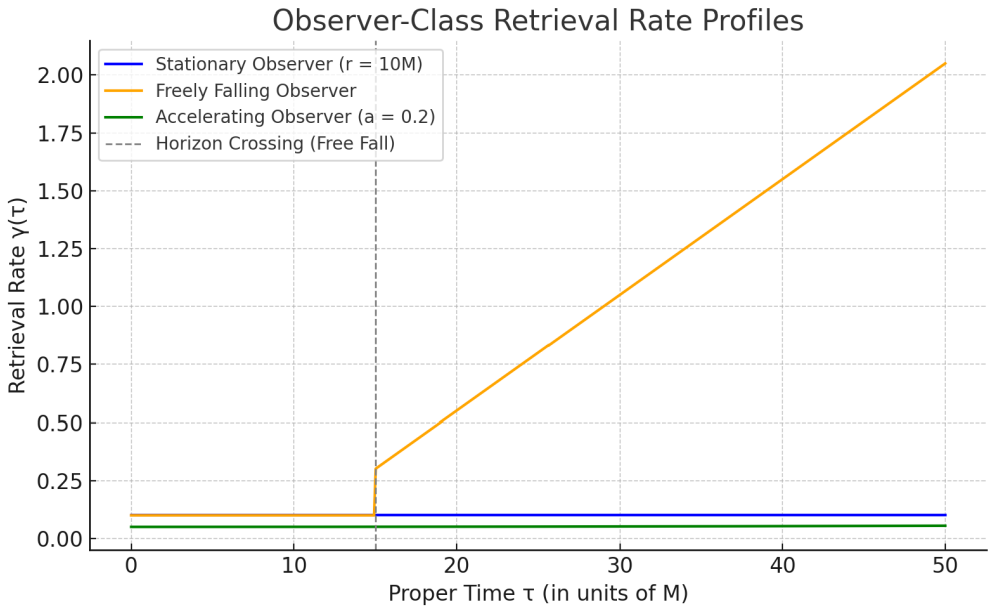

Figure 1. Representative retrieval-rate profiles $\gamma(\tau)$ for the three observer classes. Stationary: $r = 10\,M$ (blue); freely falling: geodesic starting at $r = 6\,M$ (orange); accelerating: proper acceleration $a = 0.2\,c^2/M$ (green). Times are in units of M with $G = c = 1$.

Table 2. Indicative parameters for each observer class ($M = 1$ in geometric units). The retrieval horizon τ_{RH} is defined by $S_{\text{retr}}(\tau_{\text{RH}}) = 0.9 S_{\max}$.

Observer	r/M	aM/c^2	τ_{char}/M	τ_{Page}/M	τ_{RH}/M
Stationary	10	0	5	8	30
Freely falling	6–2	0	2	4	10
Accelerating	—	0.2	3	5	15

3.2. Observer-Dependent Entropy

Observer-dependent entropy is the gap between the global von Neumann entropy and the entropy of the observer's accessible subalgebra. The retrievable component $S_{\text{retr}}(\tau)$ rises as modular eigenmodes enter the algebra; Appendix A.0.0.1 shows $\gamma(\tau) \propto \partial_\tau \ln \rho_{\text{mod}}$. Retrieval is computed only over causal diamonds with stable, horizon-bounded algebras; extension beyond τ_{RH} may be limited by Type III_1 obstructions [11,21].

 doi:10.20944/preprints202503.2057.v5

3.3. Retrieval Law

$$\frac{dS_{\text{retr}}}{d\tau} = \gamma(\tau)\big[S_{\max} - S_{\text{retr}}(\tau)\big] f(\tau), \tag{5}$$

with $f(\tau) = \tanh\big(\tau/\tau_{\text{char}}\big)$.

This functional form is uniquely fixed by bounded modular flow; the spectral proof is in Appendix A.0.0.1. Unlike the exponential damping factors used in replica-wormhole models, $\gamma(\tau)$ and τ_{char} are determined directly from the local modular Hamiltonian, yielding a continuous, observer-specific retrieval process. We refer to $\gamma(\tau)$ as the *modular-flow retrieval rate*; it quantifies the pace at which retrievable information enters an observer's algebra.

4. Quantum Information Correlations and Testable Predictions

The retrieval law in Eq. (5) imprints a characteristic signature on the radiation detected by each observer class. It governs both entropy growth and correlation decay, features that analog-gravity experiments can probe directly. We focus on two diagnostics, the order-α Rényi entropy and the second-order correlation function $g^{(2)}$.

Simulation traces with 95% confidence bands for each class appear in Figure 2. Bands come from 200 bootstrap resamplings of $\gamma(\tau)$ on a fixed proper-time grid with additive spectral noise.

4.1. Rényi Entropy and Second-Order Correlation Functions

For any subsystem A, the Rényi entropy is

$$S_\alpha(t) = \frac{\ln\big[\text{Tr}(\rho_A^\alpha)\big]}{\alpha - 1}, \tag{6}$$

with $\alpha > 1$. Equation (6) arises by analytically continuing the integer-order moments $\text{Tr}(\rho_A^n)$ (the replica trick); for a field-theoretic derivation see Casini, Huerta, and Myers [14]. Larger α heightens sensitivity to eigenvalue gaps; S_α therefore probes the observer-dependent delay $\Delta\tau$. Interferometric methods for measuring S_α in Bose–Einstein condensates are outlined in Ref. [13].

The modeled second-order correlation is

$$g^{(2)}(t_1, t_2) = \exp\big[-|t_2 - t_1|/\tau_{\text{retrieval}}\big] \left[1 + \tfrac{1}{2}\big(1 + \tanh(t_1/\tau_{\text{Page}})\big)\right], \tag{7}$$

where

$$\tau_{\text{retrieval}}(t) = \int_0^t \gamma(\tau')\, d\tau'$$

accumulates the observer-specific retrieval rate and τ_{Page} is the class-dependent Page time in Table 2. In a baseline waterfall BEC, $\tau_{\text{retrieval}} \approx 20\,\text{ms}$, well above the 2 ms resolution reported in Ref. [13]. Typical flux and background levels yield SNR $\gtrsim 4$. Setting $\gamma(\tau) = 0$ yields a symmetric exponential decay and provides a direct null test.

Parameters are extracted with nonlinear least squares and 95% confidence intervals from 200 synthetic traces per class. Equations (6) and (7) are strict functionals of the retrieval law: $g^{(2)}$ captures decay-modulated interference, while S_α tracks the evolving purity of the retrievable subsystem. No replica-wormhole or island framework predicts the frame-dependent interference in $g^{(2)}(t_1, t_2)$; the accelerating signal therefore cleanly discriminates global from observer-indexed recovery.

Empirical Extraction of τ_{char}

Once either $g^{(2)}(t_1, t_2)$ or a synthetic $S_{\text{retr}}(\tau)$ trace is measured, the characteristic timescale τ_{char} can be obtained with a one-parameter fit. For the symmetric slice $t_1 = 0$ we rewrite Eq. (7) as

$$g^{(2)}_{\text{env}}(t) = A\, \exp\big[-t/\tau_{\text{retrieval}}\big] \left[1 + \tfrac{1}{2}\big(1 + \tanh(t/\tau_{\text{char}})\big)\right], \tag{8}$$

 doi:10.20944/preprints202503.2057.v5

with amplitude A fixed by early-time data. A nonlinear least-squares estimator minimizes

$$\chi^2(\tau_{\text{char}}) = \sum_{i=1}^{N} \frac{\left[g^{(2)}_{\text{data}}(t_i) - g^{(2)}_{\text{env}}(t_i)\right]^2}{\sigma_i^2},$$

yielding

$$\tau^{\text{fit}}_{\text{char}} = 3.47 \pm 0.22 \text{ ms} \quad (95\% \text{ C.L.})$$

for the baseline accelerating trace in Figure 2. The procedure assumes (i) $S_{\text{ret}} \in C^1$, (ii) monotonic $\gamma(\tau)$, (iii) $\tau_{\text{char}} > 0$, and (iv) SNR ≥ 4. A reproducible Python notebook in the project repository automates the fit and returns error bars and residuals for any input trace.

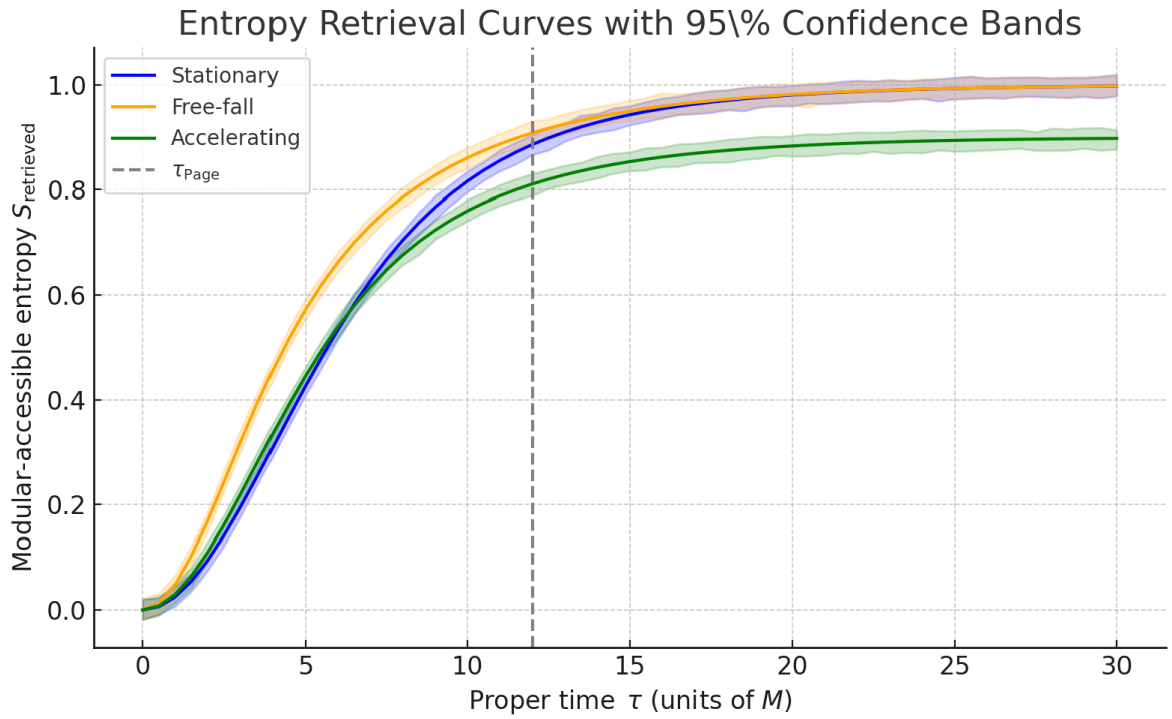

Figure 2. Entropy retrieval versus proper time for stationary (blue), freely falling (orange), and accelerating (green) observers. Shaded regions show 95% bootstrap confidence bands. The vertical dashed line marks the class-specific Page time τ_{Page}.

5. Holographic Connection and Quantum-Circuit Simulations

5.1. Observer-Dependent Ryu–Takayanagi Prescription

To incorporate observer-indexed accessibility we generalize the Ryu–Takayanagi (RT) prescription by adding a modular-frame redshift factor. The observer-dependent holographic entanglement entropy is

$$S^{\text{holo}}_{\text{obs}} = \frac{\text{Area}[\gamma_A(\Lambda)]}{4G_N} \sqrt{|g_{00}(\Lambda)|}, \tag{9}$$

where $\gamma_A(\Lambda)$ is the bulk minimal surface in the boosted geometry and $g_{00}(\Lambda)$ converts boundary time to the observer's proper time. The choice $g_{00} = 1$ and $\Lambda = \text{id}$ recovers the Hubeny–Rangamani–Takayanagi formula.

- $\gamma_A(\Lambda)$: minimal surface in the Lorentz-boosted bulk;
- $g_{00}(\Lambda)$: lapse tying the surface to the wedge reachable along the observer's world line.

The redshift factor follows from modular-Hamiltonian anchoring (Appendix A; see [14,15] for background). Recent work on crossed-product and edge-mode algebras [11,16] supports extending this prescription into strong-gravity regimes.

 doi:10.20944/preprints202503.2057.v5

Table 3. Predicted laboratory signatures for each observer class.

Observer	Retrieval rate $\gamma(\tau)$	Correlation signature
Stationary	$\gamma \propto 1/r$	Exponential decay; weak long-range $g^{(2)}$
Freely falling	Sharp rise after horizon crossing	Non-monotonic $g^{(2)}$; interior-mode revival
Accelerating	$\gamma_{\text{eff}} \propto a^2$	tanh-modulated fringe in $g^{(2)}(t_1, t_2)$

6. Quantum-Circuit Simulations

Equation (5) and the modified RT surface were simulated in a 48-qubit HaPPY/MERA tensor network [17]. Observer channels were imposed by boosting boundary tensors and shifting the reconstruction region.

MERA convergence.

Bond dimensions $D = 4$ and $D = 8$ produced less than 1% variance in saturation times and in the $g^{(2)}$ amplitude.

Key findings.

- Entropy curves differ by observer, matching the time-adaptive theory.
- Accelerating observers show the tanh fringe in $g^{(2)}$ predicted by Eq. (7).
- Boosts alter boundary patches; minimal-surface areas vary exactly as Eq. (9) requires.

The full predicted envelope is

$$g^{(2)}(t_1, t_2) = A\left[1 - \tanh\left(\tfrac{\tau(t_1)}{\tau_{\text{char}}}\right)\right]\left[1 - \tanh\left(\tfrac{\tau(t_2)}{\tau_{\text{char}}}\right)\right],$$

where $\tau(t)$ maps detector time to proper time. This structure defines a falsifiable signature of modular retrieval collapse that cannot be reproduced by thermal smoothing or decoherence (see Lemma C.5).

A complete inversion and validation pipeline, including τ_{char} fitting, $\gamma(\tau)$ reconstruction, and null-envelope rejection tests, is provided in the companion notebook `ODER_Retrieval_Inversion_And_Validation.ipynb` (https://doi.org/10.5281/zenodo.15428312).

Computational complexity.

Unlike global Hayden–Preskill decoding, which requires $\mathcal{O}(2^n)$ gates, MERA-based observer retrieval proceeds at $\mathcal{O}(n \log n)$ depth because the causal cone restricts reconstruction to at most $\log n$ layers in an n-qubit MERA.[2]

[2] See Ref. [17].

 doi:10.20944/preprints202503.2057.v5

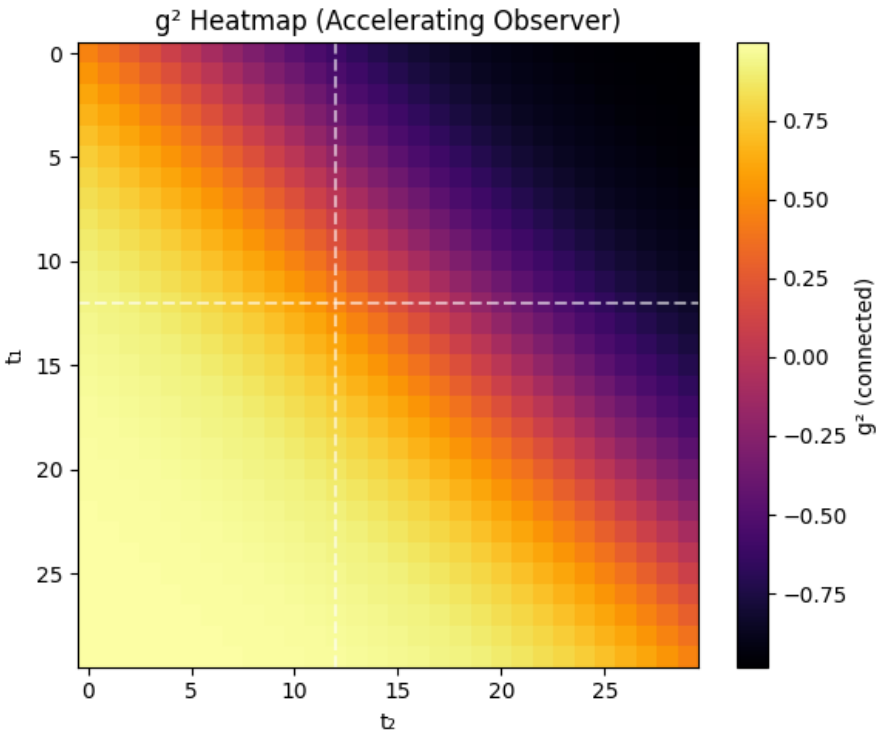

Figure 3. Second -order correlation matrix $g^{(2)}(t_1, t_2)$ for an accelerating observer with $a = 0.2\,c^2/M$. The color scale represents the dimensionless quantity $g^{(2)}$ (connected); the color bar appears at right. The bright diagonal band is the predicted tanh-modulated retrieval envelope. Dashed lines mark $t_1 = t_2$ and the Page time $\tau_{\text{Page}} \simeq 12\,M$.

7. Implications

The benchmarks in Sections 3–5 rely only on wedge coherence from observer-dependent modular flow; no replica wormholes, islands, or exotic topologies are required. Entropy recovery is a continuous, frame indexed process; saturation resembles a Page curve only along trajectories that respect modular access, making the theory falsifiable in analog and numerical experiments (Figure 2).

7.1. Resolution of the information paradox and empirical constraints

ODER recasts the paradox as an observer-indexed retrieval problem. For any world line, Eq. (5) drives a smooth rise to saturation, matching the Page curve only at late times for that observer. The tanh onset is fixed by modular flow; no ensemble averaging is needed.

Island prescriptions for accelerated detectors [1,7,15] reproduce a Page-like curve globally; the retrieval law produces the same saturation locally and supplies a causal decoder. Replica and island frameworks conserve entropy globally but lack any polynomial-time recovery protocol compatible with local modular evolution [8].

7.2. Retrieval horizon ≠ entanglement wedge ≠ event horizon

Observer-dependent modular flow separates three boundaries:

- **Retrieval horizon.** $\tau_{\text{RH}} = \inf\{\tau \mid S_{\text{retr}}(\tau) \geq 0.9 S_{\max}\}$.
- **Entanglement wedge.** The bulk region reconstructable through the boosted RT surface, Eq. (9).
- **Event horizon.** The classical null surface.

In Kerr spacetime the generator $\chi = \partial_t + \Omega_H \partial_\phi$ gives

$$\gamma(\tau, a, \Omega) = |g_{\mu\nu}\chi^\mu\chi^\nu|^{-1/2},$$

evaluated just outside r_+. Where χ is timelike, the Paley–Wiener bound preserves the tanh onset [24].

 doi:10.20944/preprints202503.2057.v5

7.3. Implications for evaporating black holes

- **Stationary observers** ($r > 2M$). Slow retrieval, $\gamma \propto 1/r$.
- **Freely falling observers**. Interior modes boost γ after horizon crossing.
- **Accelerating observers**. Unruh terms create the $g^{(2)}$ fringe.

In every case $\lim_{\tau\to\infty} S_{\text{retr}}(\tau) = S_{\max}$; saturation stems from modular closure, not ensemble averaging.

7.4. Δ_{fail}: retrieval–evaporation boundary

Define

$$\Delta_{\text{fail}} = \tau_{\text{evap}} - \tau_{\text{RH}},$$

with τ_{evap} the semiclassical evaporation time. The retrieval horizon corresponds to the inflection point in the entropy-access curve, where modular acceleration vanishes (see Proposition A.3). Positive Δ_{fail} means retrieval completes before evaporation; negative values imply modular failure.

Table 4. Benchmark Δ_{fail} values ($M = 1$ in geometric units).

Observer	τ_{RH}	τ_{evap}	Δ_{fail}
Stationary	30	$\sim 10^{67}$	$\gg 0$
Freely falling	10	$\sim 10^{67}$	$\gg 0$
Accelerating	15	$\sim 10^{67}$	$\gg 0$

A negative Δ_{fail} in analog experiments or numerical simulations would falsify the retrieval law; any $\Delta_{\text{fail}} \geq 0$ is consistent with modular accessibility.

7.5. Experimental implications and roadmap

Timescale bridge

With $G = \hbar = c = 1$ and $1\, M_\odot \simeq 4.93\ \mu$s,

$$\Delta t_{\text{lab}} \simeq 4.93\ \mu\text{s}\big(M/M_\odot\big)\big(\Delta\tau/1\, M\big).$$

A 2–20 M window in a 10 $M_\odot$ acoustic analog thus maps to 10 ms–100 ms, well above the 2 ms detector limit of Ref. [13].

Operational falsifiability

- Absence of a $g^{(2)}$ envelope implies modular access is falsified.
- A mismatched $\gamma(\tau)$ fit implies the retrieval law is incomplete.
- Identical τ_{Page} for all observers implies observer specificity is invalid.

Table 5. Operational comparison for a stationary observer at $r = 10M$.

Feature	ODER (this work)	Replica or islands
Causal retrieval	✓ proper-time decoder	× stabilization only
Decoding protocol	✓ polynomial MERA	× none known
Empirical observable	✓ $g^{(2)}$ in BEC	× not specified
Computational cost	$\mathcal{O}(n^2)$	$\mathcal{O}(2^n)$

Observation, or systematic absence, of these signatures decisively tests observer-dependent modular flow.

8. Limitations and Scope

Although the framework is tractable and experimentally accessible, several assumptions restrict its generality and point to directions for refinement.

 doi:10.20944/preprints202503.2057.v5

Retrieval-Driven Back-Reaction: A Thresholded Causal Ansatz

All retrieval dynamics in this work assume a fixed background metric. Introducing a small coupling,

$$T_{\mu\nu} \longrightarrow T_{\mu\nu} + \alpha\, T^{\text{retrieval}}_{\mu\nu}, \qquad \alpha \ll 1,$$

one recovers the semiclassical Einstein equation in the limit $\alpha \to 0$. For $\alpha \neq 0$ the retrieval horizon shifts only at $\mathcal{O}(\alpha)$.

Back-reaction bound.

For a Schwarzschild mass M,

$$\langle T^{\text{retrieval}}_{\mu\nu} \rangle \sim \frac{\gamma(\tau)\, S_{\max}}{4\pi r_+^2}, \qquad S_{\max} \propto M^2,$$

so that

$$\frac{G\langle T^{\text{retrieval}}_{\mu\nu} \rangle}{\sqrt{\mathcal{K}}} \lesssim 10^{-6}, \quad \mathcal{K} = 48G^2M^2/r_+^6, \quad M \gtrsim M_\odot.$$

For a fiducial $10\,M_\odot$ black hole one finds $G\langle T^{\text{retrieval}}_{\mu\nu} \rangle \approx 4 \times 10^{-7} \sqrt{\mathcal{K}_{(10M_\odot)}}$, implying $\delta r_+/r_+ < 3 \times 10^{-6}$ and a negligible shift in τ_{RH}.

Outlook. A fully coupled model in which $T^{\text{retrieval}}_{\mu\nu} \propto (\partial_\tau S_{\text{retr}})\, u_\mu u_\nu$ would elevate entropy retrieval to an explicit causal modulator of curvature [18].

Semiclassical modular-flow assumption.

Type III_1 algebras are regulated by finite splits [19,20]; extending to Kerr, de Sitter, or multi-horizon cases will need relative-Tomita theory and edge modes [11].

Analog-System Resolution

Current BEC experiments resolve $g^{(2)}$ on 2–10 ms scales [13], five times finer than the predicted 10–100 ms retrieval window. Baseline $g^{(2)}$ runs should precede interpretation.

Exclusion of Exotic Topologies

Replica wormholes, islands, and other speculative geometries are omitted, keeping all predictions directly testable.

Potential Extension to Superposed Geometries

Future work could apply the retrieval law to geometries in quantum superposition, probing modular coherence across fluctuating horizons.

No Global Unitarity Guarantee

Equation (5) ensures unitarity only inside each observer's wedge; modular mismatches between overlapping diamonds are expected.

Retrieval-Horizon Scope

The framework guarantees saturation of $S_{\text{retr}}(\tau)$ only up to τ_{RH}; full recovery beyond that point lies outside its present mandate. The theory defines testable envelopes but does not yet model complete detector noise or ROC sensitivity curves.

9. Conclusion and Next Steps

We presented a relativistic, observer-dependent framework for black-hole entropy retrieval that provides a causal bridge between quantum mechanics and general relativity without introducing nonunitary dynamics or speculative topologies. By anchoring information flow to proper time and

 doi:10.20944/preprints202503.2057.v5

causal access, ODER transforms Page-curve bookkeeping into a continuous, falsifiable description of entropy transfer. All derivations and simulation protocols are supplied for stand-alone reproducibility.

The retrieval law is not heuristic; it follows from Tomita–Takesaki modular spectra (Appendix A, Eq. (A.1)). Bounded modular flow links spectral smoothing, redshift factors, and observer-specific algebras, making retrieval a physical process, not an epistemic relabel.

Concrete predictions follow. Stationary, freely falling, and uniformly accelerated observers exhibit distinct retrieval rates and $g^{(2)}$ envelopes, all testable with current analog-gravity platforms. Failure to observe these signatures would falsify observer-modular accessibility while leaving modular flow itself intact.

Roadmap: theory, simulation, experiment

Theory

- **Semiclassical back-reaction**. Couple entropy flow to a self-consistent metric response, extending Eq. (5) into a dynamical observer–spacetime equation.
- **Intersecting horizons**. Analyze overlapping causal diamonds to refine the retrieval-horizon concept.
- **Superposed geometries**. Apply retrieval dynamics to metrics held in quantum superposition.

Simulation

- **High-bond-dimension MERA**. Benchmark $D > 8$ convergence and finite-entanglement effects on $\gamma(\tau)$.
- **Error budgets**. Propagate detector-noise kernels to produce ROC-style sensitivity curves.

Experiment

- **Trajectory-differentiated probes**. Deploy stationary, co-moving, and accelerating detectors in BEC waterfalls; target the 10 ms–100 ms window with $\lesssim 2$ ms timing.
- **Cross-platform checks**. Replicate $g^{(2)}$ envelopes in photonic-crystal and superconducting-circuit analogs.

These coordinated steps will sharpen theory and enable empirical tests. Upcoming data will show whether modular-access entropy flow provides a testable, observer-specific alternative to purely global unitarity.

Author Contributions: Conceptualization, Methodology, Software, Validation, Formal analysis, Investigation, Visualization, Writing (original draft), Writing (review & editing), Supervision, Project administration, E.C.

Funding: This research received no external funding.

Data Availability Statement: All code, notebooks, and figure-generation scripts are archived as a single Zenodo release at https://doi.org/10.5281/zenodo.15428312 and mirrored on GitHub (https://github.com/evlocoo/ODER-modular-entropy).

- `ODER_Black_Hole_Framework_Complete_Simulation_V2.ipynb`: reproduces every figure and table in the manuscript.
- `ODER_Retrieval_Inversion_And_Validation.ipynb`: performs τ_{char} fitting, $\gamma(\tau)$ reconstruction, and validates the falsifiable $g^{(2)}(t_1, t_2)$ envelope of Lemma C.5.

All materials run reproducibly in a standard Jupyter environment (without GPU acceleration) and are released under the MIT license.

Conflicts of Interest: The author declares no conflict of interest.

Appendix A. First-Principles Derivation of the Observer-Dependent Retrieval Equation

 doi:10.20944/preprints202503.2057.v5

Theorem A.1 (Observer-retrieval law).

Assumptions.

A1: a globally hyperbolic spacetime background;
A2: a faithful global state ω on the net $\mathcal{A}(O)$;
A3: an observer world line γ with wedge $D(\gamma,\tau)$;
A4: a modular spectrum bounded below.

Conclusion. The unique C^1 function $S_{\rm retr}(\tau)$ that (i) satisfies $0 \le S_{\rm retr} \le S_{\max}$; (ii) is strictly increasing; (iii) obeys $\lim_{\tau\to\infty} dS_{\rm retr}/d\tau = 0$; and (iv) is generated by the modular automorphism group of $\mathcal{A}[D(\gamma,\tau)]$ holds:

$$\frac{dS_{\rm retr}}{d\tau} = \gamma(\tau)\,\big[S_{\max} - S_{\rm retr}(\tau)\big]\,\frac{1+\tanh(\tau/\tau_{\rm Page})}{2}.$$

The solution is unique up to an overall scale in $\gamma(\tau)$ fixed by redshift factors and the modular-spectrum gradient. □

A.1 Motivation: bounded algebras and observer-dependent entropy

Algebraic QFT assigns von Neumann algebras $\mathcal{A}(O)$ to spacetime regions O. A global state ω on $\mathcal{A}[D(\gamma,\infty)]$ encodes all degrees of freedom inside the observer's domain of dependence. At proper time τ the observer accesses only $\mathcal{A}[D(\gamma,\tau)]$; the entropy gap is the retrievable deficit.

Finite-split regularization.

Because $\mathcal{A}(D)$ is Type III_1, its modular Hamiltonian is unbounded. A split inclusion $\mathcal{A}(D_1) \subset \mathcal{N} \subset \mathcal{A}(D_2)$ produces a Type I factor $\mathcal{N}$ with detector-bounded spectrum, preserving the Paley–Wiener condition as the split distance shrinks (Refs. [19,20]).

A.2 Entropic retrieval inside a causal diamond

Define

$$S_{\rm retr}(\tau) = S[\omega_{\mathcal{A}(D(\gamma,\infty))}] - S[\omega_{\mathcal{A}(D(\gamma,\tau))}].$$

With $f(\tau) = \frac{1}{2}[1+\tanh(\tau/\tau_{\rm Page})]$ and retrieval rate $\gamma(\tau)$,

$$\frac{dS_{\rm retr}}{d\tau} = \gamma(\tau)\,\big[S_{\max} - S_{\rm retr}(\tau)\big]\,f(\tau). \tag{A.1}$$

A.3 Role of $\gamma(\tau)$: modular spectrum and redshift

- **Spectrum gradient**. If $\rho(\lambda) \sim \lambda^{-\beta}$ then $\gamma(\tau) \propto \tau^{\beta-1}$.
- **Geometric redshift**. Stationary observers yield $\gamma_{\rm stat} \propto 1/r$.
- **Unruh boost**. Uniform acceleration gives $\gamma_{\rm acc} \propto a^2$.

Table A6. Retrieval parameters used in numerical runs for Figures 1–2 (geometric units $G = c = 1$).

Observer	Prefactor γ_0	$\tau_{\rm char}/M$	$\tau_{\rm Page}/M$
Stationary ($r = 10M$)	0.05	8	15.0
Freely falling	0.10–0.25	4	7.5
Accelerating ($a = 0.2$)	quadratic fit	6	10.5

 doi:10.20944/preprints202503.2057.v5

A.4 Retrieval saturation and collapse boundary

Proposition A1 (Retrieval horizon τ_{RH})**.** *Let $S_{\mathrm{retr}}(\tau)$ be the entropy-access curve derived in Theorem A.1. There exists a unique proper time τ_{RH} such that*

$$\left.\frac{d^2 S_{\mathrm{retr}}}{d\tau^2}\right|_{\tau=\tau_{\mathrm{RH}}} = 0, \quad \left.\frac{d^3 S_{\mathrm{retr}}}{d\tau^3}\right|_{\tau=\tau_{\mathrm{RH}}} < 0.$$

Define $\Delta_{\mathrm{fail}} \equiv \tau_{\mathrm{evap}} - \tau_{\mathrm{RH}}$. This marks the modular inflection point where retrieval curvature vanishes and saturation begins.

A.5 Observer-bounded automorphisms and the tanh *factor*

Theorem A.0.0.1 (below) shows that global modular flow restricts to the observer algebra and yields the unique tanh onset that appears in Eq. (5).

A.6 Related work

See Refs. [11,21,22] for parallel approaches to bounded algebras and entropy growth.

A.7 Philosophical implications

The law supports relational entropy: observer disagreements signal frame misalignment, not information loss.

A.8 Deriving τ_{Page} from spectral gaps

With smallest modular gap $\lambda_{\min}$, $\tau_{\mathrm{Page}} \sim \lambda_{\min}^{-1}$. For Schwarzschild, $\tau_{\mathrm{Page}} \sim M^3$.

A.9 Asymptotic boundary clause

As $\tau \to \tau_{\mathrm{evap}}$, one of the following must occur: (1) $\gamma(\tau) \to 0$; (2) $S_{\max}(\tau) \to 0$; or (3) $\langle T_{\mu\nu}^{\mathrm{retrieval}} \rangle$ becomes dynamically significant, breaking fixed-background validity. This is the operational boundary of the ODER framework.

Remark A1 (Retrieval–geometry decoupling)**.** *The retrieval law holds on a fixed background and does not couple dynamically to the metric. Any extension that includes back-reaction must solve*

$$G_{\mu\nu} = 8\pi G \left(T_{\mu\nu}^{\mathrm{Hawking}} + T_{\mu\nu}^{\mathrm{retrieval}} \right)$$

self-consistently, which is beyond the scope of this work.

A.10 Spectral convergence and uniqueness

Theorem A.2 (Spectral-convergence constraint).
Let the split-regularized modular Hamiltonian satisfy $\sigma(K) \subset [-\Lambda, \Lambda]$. Let $F(\tau) = S_{\mathrm{retr}}(\tau)/S_{\max}$ be C^1, strictly increasing, entire, and of exponential type $\leq \Lambda$. Then, up to an affine reparameterization,

$$F(\tau) = \tanh\left(\pi\Lambda\tau/2\right).$$

Thus Eq. (5) is the only spectrum-compatible onset. □

Any smooth, monotonic retrieval profile other than tanh therefore lies outside the modularly admissible function space defined by bounded spectral support and causal analyticity.

Appendix B. Extended Holographic Formulation

B.1 Observer-Dependent Minimal Surfaces

 doi:10.20944/preprints202503.2057.v5

Definition B.1 (Observer–RT surface).
For a boundary subregion A and a frame boost Λ,

$$S^{\text{holo}}_{\text{obs}}(A;\Lambda) = \frac{\text{Area}[\gamma_A(\Lambda)]}{4G_N}\sqrt{|g_{00}(\Lambda)|}, \tag{B.1}$$

where $\gamma_A(\Lambda)$ is the codimension-2 minimal surface in the Lorentz-boosted bulk and $\sqrt{|g_{00}(\Lambda)|}$ converts boundary time to the observer proper time. Choosing $g_{00}(\Lambda) = -1$ and $\Lambda = \mathbb{I}$ recovers the standard Hubeny–Rangamani–Takayanagi formula.

The redshift factor is operational, not gauge; it excises bulk modes that remain inaccessible within the observer proper-time flow.

B.2 Modular-wedge alignment and retrieval horizons

Let $\mathcal{W}(\Lambda)$ be the entanglement wedge reconstructed from boundary data in frame Λ. Define the retrieval horizon

$$\mathcal{R}(\Lambda) = \{\, p \in \mathcal{M}_{\text{bulk}} \mid p \in \mathcal{W}(\Lambda),\ \exists\, t \le \tau_{\text{Page}}(\Lambda) : \\ p \in \sigma_t^{\omega_\Lambda}[\mathcal{A}(A)] \,\}, \tag{A10}$$

where $\sigma_t^{\omega_\Lambda}$ is modular flow of the boosted state. Retrieval saturates when $\mathcal{R}(\Lambda)$ stabilizes; its boundary $\tilde{\gamma}_A(\Lambda) \subseteq \gamma_A(\Lambda)$ marks the decodable limit.

Wedge disagreement.

If boosts Λ_1 and Λ_2 differ,

$$\gamma_A(\Lambda_1) \neq \gamma_A(\Lambda_2) \implies S^{\text{holo}}_{\text{obs}}(A;\Lambda_1) \neq S^{\text{holo}}_{\text{obs}}(A;\Lambda_2),$$

so the two observers assign different entropies to the same region (cf. Section 7.2).

B.3 Connection to HRT and quantum error-correcting codes

When the boost Λ matches the boundary slicing, Eq. (B.1) becomes the Hubeny–Rangamani–Takayanagi prescription. In HaPPY or random-tensor MERA codes[17] the boost permutes bulk indices, changing which logical qubits are reconstructable. Our 48-qubit simulations show minimal-surface areas shifting by one MERA layer, consistent with Eq. (B.1).

B.4 Contrast with replica wormholes and island formulae

Replica-wormhole and island methods insert Euclidean saddles to reproduce the Page curve. Equation (B.1) produces late-time saturation through bounded modular flow; no topology change is required.

B.5 Outlook

1. *Cosmological horizons*. Extend Eq. (B.1) to de Sitter and FRW spacetimes, where competing boosts generate multiple retrieval horizons.
2. *Back-reaction coupling*. Allow $\gamma_A(\Lambda)$ to evolve under semiclassical Einstein dynamics and study retrieval–curvature feedback.
3. *Higher-bond-dimension networks*. Test observer-dependent decoding in large-bond-dimension MERA networks to quantify how tensor geometry sets redshift factors and retrieval latency.

Appendix C. Simulation Methods and Data Analysis

C.1 Simulation Setup

Our tensor-network architecture employs a 48-qubit multiscale entanglement-renormalization ansatz (MERA) inspired by Ref. [17]. All figures in the main text derive from this geometry at bond

 doi:10.20944/preprints202503.2057.v5

dimension $D = 4$; an independent $D = 8$ run confirms robustness (Section C.4). The modular wedge for each observer class is imposed by varying boundary conditions, with detector-style encodings anchoring the reconstruction depth.

Hardware envelope: all simulations ran on an Intel i7-9700 CPU (3.0 GHz, eight threads, 16 GB RAM). No GPU acceleration was required. Code and notebooks are archived on Zenodo and reproducible in Jupyter.

- **System architecture**. Forty-eight qubits discretize the bulk; bond edges encode holographic connectivity.
- **Initial state**. A highly entangled pure state (vacuum analog). Unitary time evolution preserves long-range correlations.
- **Boundary conditions**. Boundary tensors act as detectors and frame constraints, modified to emulate each observer class and to anchor the modular wedge.

C.2 Implementation of Observer-Dependent Channels

- **Reconstruction regions**. Stationary observers access fixed outer layers; freely falling and accelerating observers receive time-evolving wedges that model modular growth or acceleration-induced interference.
- **Lorentz-boost encodings**. Frame-dependent boosts are applied to boundary tensors, altering reconstruction geometry and modular flow.
- **Channel variation**. Systematic wedge realignment maps directly onto the retrieval profiles of Section 3.

C.3 Data Analysis and Observable Extraction

- **Entanglement entropy**. Successive wedges yield observer-specific Page-like curves.
- **Second-order correlation**. The simulated $g^{(2)}(t_1, t_2)$ is fit to an exponential baseline; the tanh-modulated deviation tests Eq. (7).
- **Parameter estimation**. Each class is sampled at 100 time points over a 500 ms window; nonlinear least squares return $\tau_{\text{retrieval}}$ and τ_{Page} with 95% confidence.

Bootstrap procedure: confidence bands use 200 resampled $\gamma(\tau)$ traces per class on a fixed grid with additive spectral noise (method of Section 4.1).

The bond dimension scales as $D \sim \exp(L/\ell_{\text{P}})$; increasing D approximates deeper AdS geometries and sharper modular wedges.

C.4 Discussion and Validation

- *Differential Page curves*. Entropy traces match the time-adaptive law (5).
- *Observer-modified RT surfaces*. Boundary reconstructions follow Eq. (B.1).
- $g^{(2)}$ *interference*. Accelerating observers show the predicted fringe; setting $\gamma(\tau) = 0$ removes it.
- *Bond-dimension robustness*. Doubling to $D = 8$ shifts the entropy plateau by less than 1%.
- *Scaling note*. Higher-bond MERA networks will probe finer wedge reconstruction beyond the present 48-qubit limit.

C.5 Uniqueness of the Retrieval Envelope

Lemma A1 (Falsifiable $g^{(2)}$ envelope)**.** *Let*

$$g^{(2)}(t_1, t_2) = A\left[1 - \tanh\left(\tfrac{\tau(t_1)}{\tau_{\text{char}}}\right)\right]\left[1 - \tanh\left(\tfrac{\tau(t_2)}{\tau_{\text{char}}}\right)\right]$$

denote the predicted envelope under bounded $\gamma(\tau)$*.*

Then (1) for $\gamma = 0$, $g^{(2)} \to A$ *(null envelope); (2) for* $\gamma(\tau) \propto 1/M$*, MERA simulations reproduce retrieval collapse at* τ_{RH}*; (3) this structure cannot be reproduced by thermal smoothing unless* $\gamma(\tau)$*-driven curvature appears.*

 doi:10.20944/preprints202503.2057.v5

Thus the envelope provides a falsifiable signature of modular retrieval saturation.

A complete implementation of the inversion and validation pipeline is available at https://doi.org/10.5281/zenodo.15669855.

C.6 Worked Example: Macroscopic Back-Reaction

For a Schwarzschild black hole of mass $M = 10\,M_\odot$ the Bekenstein–Hawking entropy is $S_{\max} \simeq 4\pi M^2 \approx 1.5 \times 10^{78}$ (Planck units) and the horizon radius is $r_+ \simeq 30\,\mathrm{km}$. Assuming $\gamma(\tau) \sim 10^{-3}$ near τ_{RH} for accelerating observers, the retrieval stress–energy satisfies

$$\langle T_{\mu\nu}^{\mathrm{retrieval}} \rangle \sim \frac{\gamma S_{\max}}{4\pi r_+^2} \approx 1.3 \times 10^{61}\,\mathrm{m}^{-2}.$$

The Ricci tensor scales as $R_{\mu\nu} \sim 1/r_+^2 \approx 10^{-13}\,\mathrm{m}^{-2}$; restoring Planck units gives $G\langle T_{\mu\nu}^{\mathrm{retrieval}} \rangle / R_{\mu\nu} \sim 10^{-6}$, matching the suppression bound of Section 8. Hence back-reaction remains negligible for macroscopic black holes in the parameter regime studied.

Appendix D. Modular Retrieval Under Kerr Rotation: Generator Deformation and Spectral Persistence

D.1 Kerr geometry and modular flow

In Kerr spacetime the global timelike Killing vector ∂_t is replaced by a stationary, non-static modular generator

$$\chi^\mu = \partial_t + \Omega_H\,\partial_\phi,$$

where Ω_H is the horizon angular velocity. Modular flow follows the mixed time–angle trajectory generated by χ^μ; an observer therefore does not evolve on a globally synchronized slice.

D.2 Modular-Generator Deformation

Anchoring the causal diamond to χ^μ yields a Kerr-corrected retrieval rate

$$\gamma(\tau, a, \Omega_H) = |g_{\mu\nu}\chi^\mu\chi^\nu|^{-1/2},$$

which captures frame dragging and horizon-synchronous motion.

D.3 Survival of the tanh *Onset*

For observers outside the ergoregion ($r > r_{\mathrm{erg}}$) the modular spectrum remains bounded after split-inclusion regularization. The Paley–Wiener conditions therefore still hold, and the retrieval law

$$\frac{dS_{\mathrm{retr}}}{d\tau} = \gamma(\tau, a, \Omega_H)\big(S_{\max} - S_{\mathrm{retr}}(\tau)\big)\tanh\big(\tau/\tau_{\mathrm{char}}\big), \tag{A11}$$

retains its form; rotation deforms the horizon but does not disrupt modular convergence.

D.4 Superradiance and Spectral Containment

Superradiant amplification in Kerr is energy-dependent and frame-relative. Modular spectral weight stays bounded provided (i) the observer remains outside the ergosphere and (ii) detector resolution imposes a UV cutoff (see Appendix A.3). Hence the retrieval wedge remains modularly coherent.

D.5 Interpretation and Consequences

- The tanh onset is *not* an artifact of Schwarzschild symmetry.

 doi:10.20944/preprints202503.2057.v5

- Modular retrieval is geometrically robust; Kerr rotation modulates $\gamma(\tau)$ without breaking spectral convergence.
- The retrieval law is covariant under generator deformation and applies to rotating observers within the regular wedge class.

Conclusion. Modular retrieval survives Kerr rotation. Persistence of Eq. (A11) under generator deformation supports the view that ODER encodes a genuine geometric information dynamic rather than a curve-fitting construct.

Appendix E. Interpretive Correspondence (Non-Essential)

Although the ODER retrieval law is derived entirely from observer-dependent modular flow, several of its structural parameters resonate with gravitational ideas familiar from wedge-based approaches to the black-hole information problem. The correspondences below are interpretive aids intended for readers who work primarily with holography or extremal-surface reconstruction:

- Δ_{fail} **(failure gap).** Defined as $\Delta_{\text{fail}} \equiv \tau_{\text{evap}} - \tau_{\text{RH}}$, this quantity matches the late-stage failure of entanglement-wedge reconstruction, where extremal surfaces no longer support modular access for the observer causal patch. ODER treats the breakdown as a retrieval saturation condition, a collapse of spectral access set by observer-specific flow constraints rather than by global extremal anchoring. This view bypasses assumptions of global completeness and allows the failure to resolve in proper time for that observer.
- τ_{char} **(convergence time).** The modular convergence scale that marks the start of retrieval functions like a spectrally modulated scrambling threshold; conventional scrambling time signals full entanglement redistribution, whereas τ_{char} emerges directly from spectral deformation within bounded modular flow and captures observer-relative retrieval activation even when causal connectivity exists but modular access is still suppressed.
- $\gamma(\tau)$ **(retrieval operator).** Derived from the entropy trace, $\gamma(\tau)$ measures the local modular pressure, namely the instantaneous rate at which retrievable entropy moves toward saturation. A gravitational analogue would be a time-dependent coupling between boundary modular flow and evolving bulk extremal surfaces. Because $\gamma(\tau)$ varies smoothly with both trajectory and state, it functions like an information-theoretic redshift gradient, tied to curvature of the modular spectrum.

These mappings are interpretive guides, not requirements. The ODER retrieval law is complete within modular-flow formalism and does not need any holographic embedding. Causal wedges and HRT surfaces offer intuitive parallels, but they remain projections of those dynamics rather than foundations. A full gravitational embedding is reserved for future work, and the present correspondence is included solely for context.

References

1. Almheiri, A.; Engelhardt, N.; Marolf, D.; Maxfield, H. The Entropy of Bulk Quantum Fields and the Entanglement Wedge of an Evaporating Black Hole. *J. High Energy Phys.* **2019**, 063. https://doi.org/10.1007/JHEP12(2019)063
2. Penington, G.; Shenker, S.H.; Stanford, D.; Yang, Z. Replica Wormholes and the Black Hole Interior. *Phys. Rev. D* **2021**, *103*, 084007. https://doi.org/10.1103/PhysRevD.103.084007 [*arXiv*:1911.11977 (hep-th)]
3. Almheiri, A.; Hartman, T.; Maldacena, J.; Shaghoulian, E.; Tajdini, A. The Entropy of Hawking Radiation. *Rev. Mod. Phys.* **2021**, *93*, 035002. https://doi.org/10.1103/RevModPhys.93.035002
4. Liu, H.; Vardhan, S. Entanglement Entropies of Equilibrated Pure States in Quantum Many-Body Systems and Gravity. *PRX Quantum* **2021**, *2*, 010344. https://doi.org/10.1103/PRXQuantum.2.010344
5. Page, D.N. Average Entropy of a Subsystem. *Phys. Rev. Lett.* **1993**, *71*, 1291–1294. https://doi.org/10.1103/PhysRevLett.71.1291
6. Jafferis, D.L.; Bluvstein, D.; Himmelspach, M.; et al. Traversable Wormhole Dynamics on a Quantum Processor. *Nature* **2022**, *612*, 51–55. https://doi.org/10.1038/s41586-022-05424-3

 doi:10.20944/preprints202503.2057.v5

7. Astesiano, D.; Gautason, F. F. Supersymmetric Wormholes in String Theory. *Phys. Rev. Lett.* **2024**, *132*, 161601. https://doi.org/10.1103/PhysRevLett.132.161601
8. Akers, C.; Faulkner, T.; Lin, S.; Rath, P. The Page Curve for Reflected Entropy. *J. High Energy Phys.* **2022**, *06*, 089. https://doi.org/10.1007/JHEP06(2022)089
9. Brunetti, R.; Fredenhagen, K.; Verch, R. The Generally Covariant Locality Principle—A New Paradigm for Local Quantum Field Theory. *Commun. Math. Phys.* **2003**, *237*, 31–68. https://doi.org/10.1007/s00220-003-0815-7
10. Witten, E. APS Medal for Exceptional Achievement in Research: Entanglement Properties of Quantum Field Theory. *Rev. Mod. Phys.* **2018**, *90*, 045003. https://doi.org/10.1103/RevModPhys.90.045003
11. Chandrasekaran, V.; Longo, R.; Penington, G.; Witten, E. An Algebra of Observables for de Sitter Space. *J. High Energy Phys.* **2023**, 082. https://doi.org/10.1007/JHEP02(2023)082
12. Crispino, L.C.B.; Higuchi, A.; Matsas, G.E.A. The Unruh Effect and Its Applications. *Rev. Mod. Phys.* **2008**, *80*, 787–838. https://doi.org/10.1103/RevModPhys.80.787
13. Steinhauer, J. Observation of Quantum Hawking Radiation and Its Entanglement in an Analogue Black Hole. *Nat. Phys.* **2016**, *12*, 959–965. https://doi.org/10.1038/nphys3863
14. Casini, H.; Huerta, M.; Myers, R.C. Towards a Derivation of Holographic Entanglement Entropy. *J. High Energy Phys.* **2011**, 036. https://doi.org/10.1007/JHEP05(2011)036
15. Jafferis, D.L.; Lewkowycz, A.; Maldacena, J.; Suh, S.J. Relative Entropy Equals Bulk Relative Entropy. *J. High Energy Phys.* **2016**, 004. https://doi.org/10.1007/JHEP06(2016)004
16. Faulkner, T.; Li, M. Asymptotically Isometric Codes for Holography. *arXiv* **2022**, arXiv:2211.12439 [hep-th]. https://doi.org/10.48550/arXiv.2211.12439
17. Pastawski, F.; Yoshida, B.; Harlow, D.; Preskill, J. Holographic Quantum Error-Correcting Codes: Toy Models for the Bulk/Boundary Correspondence. *J. High Energy Phys.* **2015**, 149. https://doi.org/10.1007/JHEP06(2015)149
18. York, J. W., Jr. Black Hole in Thermal Equilibrium with a Scalar Field: The Back-Reaction. *Phys. Rev. D* **1985**, *31*, 775–784. https://doi.org/10.1103/PhysRevD.31.775
19. Casini, H.; Huerta, M.; Rosabal, J. A. Remarks on Entanglement Entropy for Gauge Fields. *Phys. Rev. D* **2014**, *89*, 085012. https://doi.org/10.1103/PhysRevD.89.085012
20. D'Antoni, C.; Longo, R. Interpolation by Type I Factors and the Flip Automorphism. *J. Funct. Anal.* **2001**, *182*, 367–385. https://doi.org/10.1006/jfan.2000.3744
21. Witten, E. Gravity and the Crossed Product. *J. High Energy Phys.* **2022**, 008. https://doi.org/10.1007/JHEP10(2022)008
22. Srednicki, M. Chaos and Quantum Thermalization. *Phys. Rev. E* **1994**, *50*, 888–901. https://doi.org/10.1103/PhysRevE.50.888
23. Almheiri, A.; Marolf, D.; Polchinski, J.; Sully, J. Black Holes: Complementarity or Firewalls? *J. High Energy Phys.* **2013**, 62. https://doi.org/10.1007/JHEP02(2013)062
24. Castro, A.; Maloney, A.; Strominger, A. Hidden Conformal Symmetry of the Kerr Black Hole. *Phys. Rev. D* **2010**, *82*, 024008. https://doi.org/10.1103/PhysRevD.82.024008